
Analyzing the Training Dynamics of Image Restoration Transformers: A Revisit to Layer Normalization

MinKyu Lee, Sangeek Hyun, Woojin Jun, Hyunjun Kim, Jiwoo Chung, Jae-Pil Heo*
Sungkyunkwan University

{2minkyulee, hse1032, junwoojinjin, arithu3, jiwoo.jg, jaepilheo}@gmail.com

Abstract

This work investigates the internal training dynamics of image restoration (IR) Transformers and uncovers a critical yet overlooked issue: conventional LayerNorm leads feature magnitude divergence, up to a *million scale*, and collapses channel-wise entropy. We analyze this phenomenon from the perspective of networks attempting to bypass constraints imposed by conventional LayerNorm due to conflicts against requirements in IR tasks. Accordingly, we address two misalignments between LayerNorm and IR tasks, and later show that addressing these mismatches leads to both stabilized training dynamics and improved IR performance. Specifically, conventional LayerNorm works in a per-token manner, disrupting spatial correlations between tokens, essential in IR tasks. Also, it employs an input-independent normalization that restricts the flexibility of feature scales, required to preserve input-specific statistics. Together, these mismatches significantly hinder IR Transformer’s ability to accurately preserve low-level features throughout the network. To this end, we introduce Image Restoration Transformer Tailored Layer Normalization (*i*-LN), a surprisingly simple drop-in replacement for conventional LayerNorm. We propose to normalize features in a holistic manner across the entire spatio-channel dimension, preserving spatial relationships among individual tokens. Additionally, we introduce an input-adaptive rescaling strategy that maintains the feature range flexibility required by individual inputs. Together, these modifications effectively contribute to preserving low-level feature statistics of inputs throughout IR Transformers. Experimental results verify that this combined strategy enhances both the stability and performance of IR Transformers across various IR tasks.

1 Introduction

Image restoration (IR) is a fundamental challenge in computer vision that aims to reconstruct high-quality images given degraded inputs. With the success of Vision Transformers [9], Transformer-based architectures have been actively adopted for IR tasks, where models such as SwinIR [19] have shown clear advantages over convolutional networks. As a result, Transformer-based architectures have become a common backbone in IR. However, despite recent architectural advances, the underlying training dynamics of IR Transformers remain underexplored.

In this paper, we take a closer look at their internal behavior and uncover a critical yet overlooked phenomenon: feature magnitudes diverge dramatically, reaching scales up to a *million*, while channel-wise feature entropy drops sharply (Fig.1). Interestingly, this observation aligns with findings from previous studies [29, 17], which similarly reported visual artifacts and unstable training when networks attempt to bypass normalization layers by amplifying feature values.

Building on these insights, we hypothesize that the observed feature divergence in IR Transformers arises from networks attempting to circumvent the constraints of LayerNorm that do not align with

*Corresponding author.

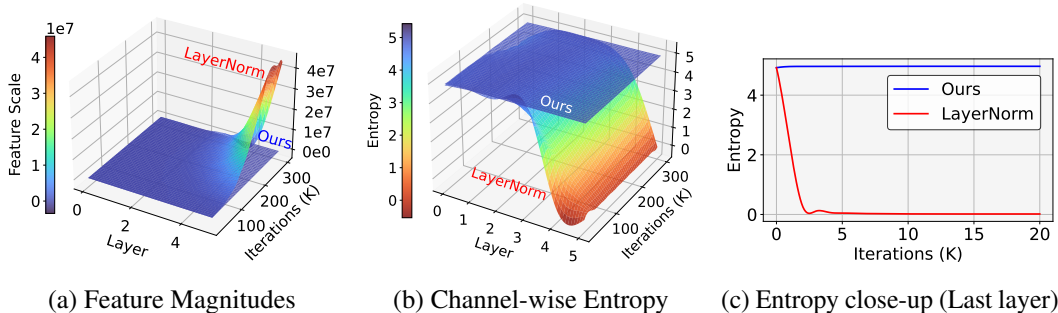


Figure 1: **Visualization of feature magnitudes and channel-wise entropy during training of an Image Restoration (IR) Transformer using conventional LayerNorm (LN) and *i*-LN (Ours).** (a) Evolution of feature magnitudes across layers and training iterations, highlighting the dramatic divergence (to million-scale) under conventional LN. (b) Channel-wise entropy. LN shows extremely low entropy values, indicating acute peaks hidden in specific channels. Ours exhibits significant stability, representing well-distributed activation across channels. (c) Entropy behavior of the last layer during early training iterations. This reveals that entropy drops sharply at the very early stage under conventional LN. In contrast, our *i*-LN consistently maintains higher and stable entropy, supporting healthier training dynamics.

the characteristics of IR tasks. Accordingly, we identify two key mismatches between LayerNorm and IR tasks; and later demonstrate that addressing these leads to both stabilized feature statistics and substantial performance gains. First, LayerNorm operates in a per-token manner, without considering inter-pixel (token) relationships. This disrupts the spatial correlations in input features, an aspect crucial for high-fidelity image restoration. Second, it maps intermediate features into a unified normalized space, limiting the range flexibility of internal representations. This thereby disregards the input-dependent statistical variability [21] that is inherent in IR tasks. Together, these mismatches significantly hinder IR Transformer’s ability to accurately preserve low-level features throughout the network, which is necessary for faithful image restoration. While one intuitive solution could be the complete removal of normalization layers [21, 29, 17, 16], our experimental observations highlight significant training instability when normalization is entirely omitted from IR Transformers (Tab.1).

In this work, we show that these issues can be addressed in a surprisingly simple manner. We propose the *Image Restoration Transformer Tailored Layer Normalization (i-LN)*, which acts as a drop-in replacement to conventional (vanilla) LayerNorm by better aligning with the unique requirements of IR tasks. Instead of normalizing each token independently, we propose to apply normalization across the entire spatio-channel dimension within IR Transformers (Fig.2). This holistic approach preserves spatial relationships among tokens, contrary to vanilla LayerNorm, which disrupts critical correlations induced by the per-token operational aspect. Furthermore, by rescaling features with the normalization parameters after each attention and feed-forward layer, we explicitly account for input-dependent variations in internal feature statistics. This tailored strategy enables intermediate features to retain input-specific statistical characteristics, thereby preserving both input dependency and range flexibility. Together, these modifications effectively preserve low-level feature statistics throughout the network, enabling IR Transformers to better restore high-quality images.

Extensive experiments demonstrate that simply replacing conventional LayerNorm with *i*-LN effectively stabilizes training dynamics and also leads to substantial performance gains across various IR tasks. Additionally, we observe cues suggesting improved spatial correlation modeling, and the resulting models are also notably more robust under reduced-precision inference.

2 Related Work

Image Restoration Transformers. Recent advances in Image Restoration (IR) transformers [5, 32, 30, 35] show superior performance over CNNs [8, 18, 38] by leveraging attention mechanisms to effectively model long-range context. A pioneering work, SwinIR [19], adopted an efficient Swin-Transformer [22] based architecture in IR tasks, balancing computational cost and restoration quality. A notable method is HAT, which originated as a super-resolution model [7] but expanded to general image restoration tasks [6]. By unifying spatial and channel attention within a hybrid attention

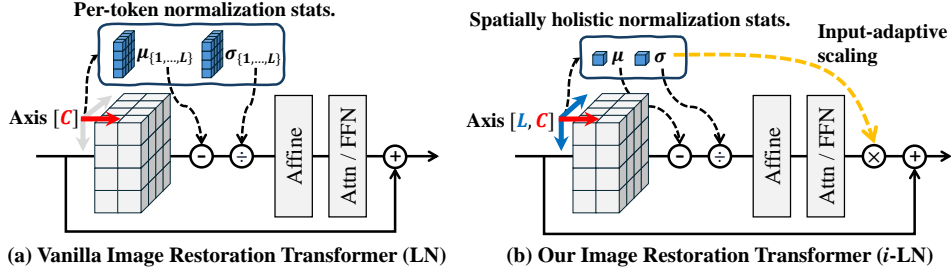


Figure 2: Comparison of IR Transformer blocks using conventional LayerNorm (LN) and our proposed Image Restoration Transformer Tailored Layer Normalization (*i*-LN). Unlike conventional LN, which normalizes each token independently, *i*-LN applies holistic normalization across the entire spatio-channel dimension, preserving essential spatial correlations between tokens. Additionally, *i*-LN introduces an input-dependent rescaling of features after the attention (Attn) and feedforward (FFN) layers, maintaining feature range flexibility. These together enable IR Transformers to preserve low-level characteristics of input throughout the network, aligning with unique requirements of IR.

framework, HAT surpasses existing IR Transformers in both restoration fidelity and robustness across various IR tasks. Building on these advancements, we adopt representative IR transformers, SwinIR and HAT as the backbone architecture for analysis throughout this work.

Abnormal Feature Behaviors in Deep Networks. Normalization is a key element in enhancing stability and performance in deep networks, but also can lead to unintended feature behavior. EDSR [21], which is a foundational work in super-resolution pointed out that BatchNorm removes range flexibility of intermediate features, leading to a performance drop. Accordingly, normalization layers are removed in the most recent CNN-based SR architectures. Meanwhile, ESRGAN [29] and StyleGAN2 [17] observe that InstanceNorm and BatchNorm, respectively, cause water droplet-like artifacts. They suggest that the generator might learn to deceive feature statistics by sneaking abnormal values in internal features to reduce the effects of normalization. EDM2 [16] identifies feature magnitude divergence in diffusion models. Accordingly, they redesign the network architecture to preserve the magnitude based on statistical assumptions, leading to overall performance enhancement. DRCT [12] notes that feature map intensities drop sharply at the end of SR networks, finding that addressing abnormal feature scale may lead to improved performance.

3 Method

3.1 Observation

Abnormal Feature Statistics. Our initial analysis focuses on tracking the trajectory of internal feature scales during the training of IR Transformers. Following the conventions [16], we visualize the squared mean of intermediate features at each basic building block of the network. We select the x4 SR task using the HAT [6] model as a representative IR task (Fig.1).

The analysis reveals that feature statistics diverge dramatically, reaching values up to a *million* scale. To pinpoint the origins of this feature divergence, we analyze the feature entropy across the channel-axis. Analysis demonstrates a sharp decrease in feature entropy, which indicates the presence of channels with extreme values that dominate the statistics. Since these extreme values are unusual, this motivates us to further investigate. Accordingly, we analyze the training dynamics across configurations by varying the network scale (Fig.3a3b), varying the IR tasks (Fig.3c), and varying the normalization scheme (Fig.5); and observe that this phenomenon occurs across all configurations utilizing standard IR Transformers. Notably, this type of abnormal peaky values hidden across the channel dimension aligns with the findings in prior studies [17, 29, 28], which have discussed how neural networks sneak peaky values to bypass normalization.

Inspired by prior observations, we hypothesize the root cause of this feature divergence as the mismatch between IR tasks and constraints raised by LayerNorm. Specifically, we point out the following two operations in LayerNorm: 1) the per-token operational scheme, which disrupts inter-token spatial correlations in network features, and 2) the input-blind mapping towards a unified normalized space, disregarding the unique statistical properties of the input. Overall, since constraints of LayerNorm conflict with important requirements in IR tasks, the network amplifies values in specific channels as an attempt to bypass LayerNorm (Sec.4.2.4).

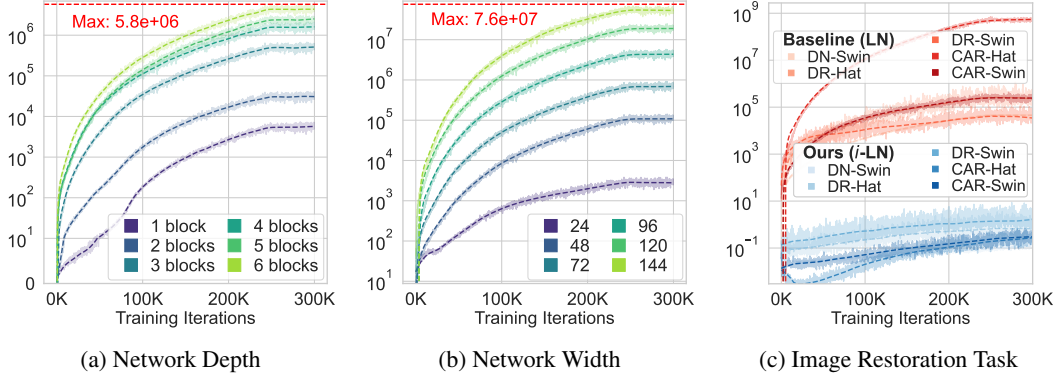


Figure 3: **Analysis of feature divergence behavior in IR Transformers across different settings.** (a-b) Feature divergence signifies as the network scales. (c) Feature divergence appears across various Transformer backbones and IR tasks: super-resolution (SR), denoising (DN), deraining (DR), JPEG compression artifact removal (CAR), demonstrating that this phenomenon is widespread but can be effectively mitigated by replacing conventional LayerNorm with the proposed *i*-LN.

3.2 Tailoring LayerNorm for Image Restoration Transformers

Baseline. Conventional Transformer architectures utilize the per-token LayerNorm (LN) as the de facto normalization scheme. Specifically, it manipulates the feature statistics as follows:

$$\mu_l = \mathbb{E}_c[x_{l,c}], \quad \sigma_l^2 = \mathbb{E}_c[(x_{l,c} - \mu_l)^2], \quad (1)$$

$$\text{LN}(x_l) = \gamma \frac{1}{\sqrt{\sigma_l^2 + \epsilon}} (x_l - \mu_l) + \beta, \quad (2)$$

where $x_{l,c} \in \mathbb{R}^1$ is the c^{th} channel of l^{th} token for input feature $x \in \mathbb{R}^{L \times C}$ and the expectation $\mathbb{E}_c[\cdot]$ is taken over the channel dimension c , and $\gamma, \beta \in \mathbb{R}^c$ are each channel-wise affine transformation parameters. As discussed above, vanilla LayerNorm normalizes each token individually, neglecting inter-token spatial relationships and input-dependency of feature statistics.

To this end, we propose the Image Restoration Transformer Tailored LayerNorm (*i*-LN), which better reflects the characteristics of IR tasks, acting as a direct drop-in replacement for conventional LayerNorm. Later, we provide extensive experimental results validating the effectiveness of *i*-LN, in terms of stabilizing training dynamics, and consistent performance gain across various IR tasks.

Spatially Holistic Normalization. We propose a simple variant of LayerNorm that improves in preserving inter-token spatial relationships of input features. Instead of normalizing each token individually, we derive normalization statistics from the entire spatio-channel dimension of the feature, indicated as LN*, as follows:

$$\mu = \mathbb{E}_{l,c}[x_{l,c}], \quad \sigma^2 = \mathbb{E}_{l,c}[(x_{l,c} - \mu)^2], \quad (3)$$

$$\text{LN}^*(x) = \gamma \frac{1}{\sqrt{\sigma^2 + \epsilon}} (x - \mu) + \beta, \quad (4)$$

where the expectation $\mathbb{E}_{l,c}[\cdot]$ is taken over both spatial (l) and channel dimensions (c). This straightforward modification effectively mitigates the issue raised by the per-token operation in vanilla LayerNorm, leading to stabilized feature scale.

Preserving Input Dependent Statistics. We further tailor LayerNorm to better suit the requirements of IR tasks. Specifically, we address the issue of input-blind normalization. While IR tasks require the preservation of input-dependent feature statistics for faithful reconstruction, conventional LayerNorm in IR Transformers overlooks this aspect by mapping features into a unified normalized space. Although normalization improves training stability, it also causes the model to lose critical input-dependent information by restricting the range flexibility of internal representations [21].

Accordingly, we propose a simple rescaling strategy that effectively tackles this issue. We rescale the output of attention and feed-forward networks by their standard deviation computed in the preceding

Idx	Method	SC	Set5		Set14		BSD100		Urban100		Manga109	
			PSNR	SSIM								
1	LayerNorm	✗	32.51	.8992	28.79	.7876	27.68	.7411	26.55	.8015	31.01	.9150
2	LayerScale	✗	32.53	.8997	28.89	.7887	27.76	.7426	26.75	.8058	31.37	.9178
3	RMSNorm	✗	32.60	.9001	28.88	.7879	27.74	.7417	26.67	.8037	31.24	.9165
4	ReZero	✓	32.46	.8979	28.81	.7861	27.70	.7406	26.41	.7964	31.05	.9147
5	None	✓	-	-	-	-	-	-	-	-	-	-
6	InstanceNorm	✓	32.63	.9010	28.98	.7907	27.80	.7445	27.02	.8136	31.46	.9199
7	BatchNorm [†]	✓	32.62	.9004	28.95	.7901	27.80	.7442	26.70	.8123	31.39	.9186
8	<i>i</i> -LN (Ours)	✓	32.72	.9019	29.01	.7915	27.84	.7456	27.17	.8167	31.82	.9228

Table 1: **Quantitative evaluation of various normalization schemes for $\times 4$ SR (HAT).** [†] indicates evaluated in train-mode. SC indicates spatial consistency of the normalization scheme. Best results in **bold**.

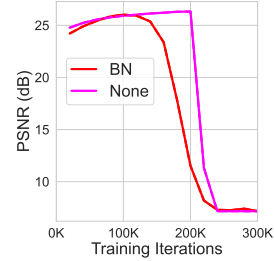


Figure 4: Eval-mode BatchNorm (BN) and removing all normalization (None) fails to converge.

normalization process as the yellow line in Fig.2b. Accordingly, a typical Transformer layer could be improved as follows:

$$x^{i+1} = x^i + \sqrt{(\sigma^i)^2 + \epsilon} \cdot f(\text{LN}^*(x^i)) \quad (5)$$

where f indicates either the variants of attention (Attn) or feedforward (FFN) layers, x^i and σ^i are features and the corresponding standard-deviation at block index i . Overall, this acts as an input-adaptive scaling, allowing range flexibility of features. This simple strategy enables IR Transformers to better preserve the per-instance statistics throughout the network, leading to overall improved IR performance. We refer to this integrated strategy as *i*-LN in the following sections.

4 Experiments

4.1 Experimental Setup

Training Settings. Since recent works have discrepancies in their detailed training settings [5], we reimplement baseline methods and our method under identical settings for fair comparison. Networks for deraining (DR) were trained on Rain13K [15], while DF2K (DIV2K [1] + Flickr2K [20]) was used for other tasks. Only geometric augmentations (random flips, rotations, crops) were applied, without mixing augmentations, progressive patch sizing, or warm-start scaling. We used the Adam optimizer with lr=2e-4 for 300K iterations. The training patch sizes is: 128×128 for $\times 4$ super-resolution (SR) and DR; 64×64 for denoising (DN), JPEG compression artifact removal (CAR), and $\times 2$ SR. Representative IR Transformers used are SwinIR [19], HAT [6], and DRCT [12].

Evaluation Settings. Standard benchmarks are employed including: Set5 [4], Set14 [33], BSD100 [23], Urban100 [13], Manga109 [24] for SR; CBSD68 [23], Kodak [11], McMaster [37], Urban100 for DN; LIVE1 [25], Classic5 [10], Urban100 [13] for CAR; Test100 [36] and Rain100L [31] for DR. We crop Urban100 into non-overlapping 256×256 sub-patches due to memory limits for CAR and DN. We report PSNR and SSIM indices. Experiments were performed on NVIDIA A6000s.

4.2 Analysis

4.2.1 Analysis Under Normalization Scheme Variation

We analyze the effects of various normalization techniques, including representative normalization schemes as vanilla LayerNorm (LN) [2], per-token RMSNorm (RMS) [34], InstanceNorm (IN) [27], BatchNorm (BN) [14], and our proposed *i*-LN. Considering previous studies where completely removing normalization from SR networks [21, 29] led to performance improvements, we additionally tested a similar configuration indicated as *None*, where we remove all normalization layers.

Further, we investigate the empirical impacts of recent methods designed to stabilize Transformer training: ReZero (RZ) [3] and LayerScale (LS) [26]. ReZero removes LayerNorm from Transformer blocks and multiplies a learnable zero-initialized scalar to the residual path. Similarly, LayerScale multiplies a near-zero-initialized learnable diagonal matrix to the residual path but reintroduces LayerNorm. Since both methods initially multiply a (near) zero-scale factor to the network output, we consider them as potential solutions to resolve the feature increasing issue in IR tasks. Notably, these methods also align with prior studies in SR [21, 29], where multiplying a small scale factor to the residual path components helped the network to converge. Overall, this study aims to explore

Table 2: **Quantitative comparison between the conventional LayerNorm (LN) and our proposed i -LN across diverse IR tasks.** We evaluate PSNR and SSIM indices on representative benchmarks. All experiments have been reproduced under identical training settings to ensure fair comparison. The best result for each setting is highlighted in **bold**.

Backbone	Scale	Set5		Set14		BSD100		Urban100		Manga109		Backbone	Testset	Metric	
		PSNR	SSIM			PSNR	SSIM								
HAT + LN	$\times 2$	38.14	.9610	33.78	.9196	32.19	.9000	32.16	.9297	38.84	.9778	HAT + LN	Rain100L	34.35	.9471
HAT + i -LN	$\times 2$	38.37	.9619	34.08	.9218	32.42	.9028	33.32	.9385	39.69	.9794	HAT + i -LN		36.20	.9641
DRCT + LN	$\times 2$	38.19	.9613	33.28	.9197	32.28	.9010	32.60	.9323	39.23	.9785	SwinIR + LN	Rain100L	33.00	.9434
DRCT + i -LN	$\times 2$	38.23	.9614	33.86	.9206	32.31	.9014	32.79	.9344	39.40	.9788	SwinIR + i -LN		34.43	.9527
HAT + LN	$\times 4$	32.51	.8992	28.79	.7876	27.68	.7411	26.55	.8015	31.01	.9150	HAT + LN	Test100	29.52	.8905
HAT + i -LN	$\times 4$	32.72	.9019	29.01	.7915	27.84	.7456	27.17	.8167	31.82	.9228	HAT + i -LN		30.14	.9022
DRCT + LN	$\times 4$	32.50	.8989	28.85	.7871	27.73	.7414	26.63	.8021	31.24	.9169	SwinIR + LN	Test100	27.45	.8766
DRCT + i -LN	$\times 4$	32.57	.8997	28.91	.7887	27.76	.7426	26.79	.8063	31.41	.9188	SwinIR + i -LN		29.87	.8982

(a) Single image super-resolution (SR)

(b) Image deraining (DR)

Backbone	σ	Urban100	CBS68	Kodak24	McMaster	Backbone	q	Urban100		LIVE1		Classic5	
		PSNR	PSNR	PSNR	PSNR			PSNR	SSIM	PSNR	SSIM	PSNR	SSIM
HAT + LN	15	35.489	34.285	35.347	35.440	HAT + LN	10	28.45	.8514	27.89	.8048	29.94	.8167
HAT + i -LN	15	35.558	34.296	35.366	35.477	HAT + i -LN	10	28.52	.8530	27.90	.8057	29.96	.8178
SwinIR + LN	15	35.077	34.164	35.147	35.183	SwinIR + LN	10	27.86	.8400	27.65	.7995	29.72	.8111
SwinIR + i -LN	15	35.138	34.181	35.177	35.223	SwinIR + i -LN	10	27.92	.8410	27.62	.7993	29.72	.8111
HAT + LN	25	33.296	31.622	32.864	33.105	HAT + LN	40	33.26	.9302	32.63	.9158	34.34	.9060
HAT + i -LN	25	33.384	31.632	32.887	33.139	HAT + i -LN	40	33.36	.9312	32.67	.9162	34.39	.9066
SwinIR + LN	25	32.753	31.480	32.643	32.829	SwinIR + LN	40	32.62	.9245	32.34	.9127	34.11	.9036
SwinIR + i -LN	25	32.803	31.489	32.660	32.848	SwinIR + i -LN	40	32.68	.9252	32.35	.9129	34.12	.9038

(c) Color image denoising (DN)

(d) Image JPEG compression artifact removal (CAR)

1) the feature divergence tendency of per-token and holistic normalizations and 2) determine which normalization method yields the best performance.

Feature Divergence Behavior. Fig.5 illustrates that feature divergence always emerges when using per-token normalizations: vanilla LN, RMSNorm, and LayerScale. In contrast, spatially consistent normalizations as our i -LN or BN, IN, ReZero do not exhibit the divergence trend. For the configuration without any normalization, we observe failure to converge due to unstable training. However, the feature magnitudes are well-bounded before this failure occurs, aligning with other normalization schemes without the per-token operation. This observation also aligns with our hypothesis that the feature divergence phenomena is closely related to the per-token normalization, and also reveals that any spatially consistent normalization could potentially reduce this effect.

Performance Comparisons. We further analyze the empirical performance for each normalization scheme in Tab.1. Conventional LayerNorm performs the worst since it neglects inter-token spatial relationships and maps features into a unified normalized space, disregarding the input-dependent desirable feature statistics. LayerScale and RMSNorm show improvement against vanilla LN, but perform worse than methods with spatially consistent normalization. Meanwhile, for the configurations without any normalization (None), the network fails to converge potentially due to unstable gradients raised by the absence of normalization, similar to prior studies in RZ [3]. BN leads to a significant performance drop in eval-mode, despite being healthy in train-mode; consistent with prior studies [21, 28]. This signifies the necessity of per-image statistics within the normalization scheme for IR tasks. InstanceNorm performs better than vanilla LayerNorm but worse than ours, similar to train-mode BatchNorm. Both InstanceNorm and BatchNorm discard crucial channel-wise information necessary for representing deep features, resulting in limited performance. However, despite these limitations in current spatially consistent normalization schemes (IN, BN), they already outperform those with per-token normalization schemes (LN, LS, RMS). Meanwhile, our i -LN achieves the best performance among all examined methods, demonstrating its effectiveness in preserving important inter-token spatial relationships and internal statistics, and ultimately the input low-level features throughout the network.

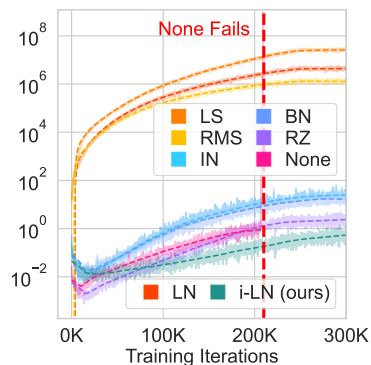


Figure 5: Feature divergence analysis across various normalizations.

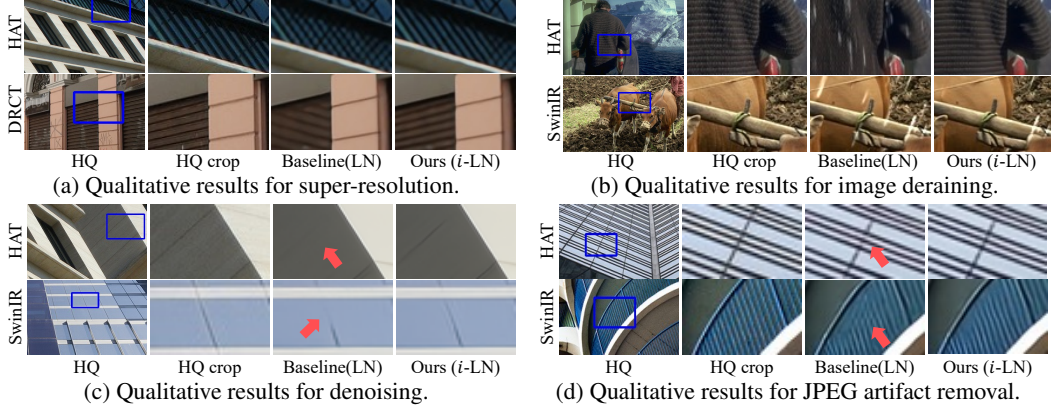


Figure 6: Qualitative comparison across four representative image restoration tasks.

4.2.2 Analysis Under Task Variation

Feature Divergence Behavior. Fig. 3c illustrates the evolution of feature magnitudes across various Image Restoration (IR) tasks, including Image Super-Resolution (SR), Image Denoising (DN), Image Deraining (DR), and JPEG Compression Artifact Removal (CAR). The figure clearly demonstrates that feature divergence consistently occurs across all restoration tasks under conventional LayerNorm. In contrast, integrating our *i*-LN effectively resolves this issue, maintaining stable and well-bounded feature scales throughout training. This consistent stabilization of internal feature magnitudes confirms the general applicability and robustness of our proposed method across diverse IR scenarios.

Benchmark: Image Super-Resolution (SR). Tab.2a and Fig.6a illustrate quantitative and qualitative results for SR. Compared to vanilla LayerNorm, we achieve significant improvements across benchmarks. Notably, SR benefits greatly from our method due to the inherent nature of SR: the input is entirely reliable, since it exactly aligns with the low-frequency information in the ground truth. By precisely preserving these input features, our method substantially enhances restored image quality.

Benchmark: Image Deraining (DR). Similarly, Tab. 2b and Fig. 6b demonstrate substantial improvements of our method in image deraining compared to conventional LayerNorm. This improvement is particularly pronounced because our method effectively preserves reliable input regions, specifically the local areas unaffected by rain streaks. By explicitly maintaining these local correspondences with the ground truth, our *i*-LN method achieves improved restoration accuracy.

Benchmark: Image Denoising (DN) Tab. 2c and Fig. 6c demonstrate that our method consistently outperforms conventional LayerNorm in image denoising tasks. However, the observed performance improvements are smaller compared to SR and Deraining. This relatively reduced benefit arises because denoising involves uniformly distributed corruptions across the entire image, limiting the advantage gained from explicitly preserving particular input features. Despite this, visual examples confirm meaningful improvements in recovering sharp edges.

Benchmark: JPEG compression artifact removal (CAR). Similarly, Tab. 2d and Fig. 6d demonstrate consistent improvements of our method over LayerNorm for JPEG compression artifact removal. However, these performance gains remain smaller than those achieved in SR and Deraining. Similar to denoising, JPEG artifacts affect images globally and irregularly, limiting the advantage of explicitly preserving specific input details. Still, visual examples illustrate consistent improvement in accurate artifact reductions, highlighting our method’s broad effectiveness across various IR tasks.

4.2.3 Impact of Network Scale

We further investigate how the network size affects feature divergence by varying the depth and width of the IR Transformer, and observe a clear positive correlation (Fig.3a-3b). This highlights that larger networks may be more susceptible to this issue. On the other hand, analysis has shown that only a few channels contribute to the abnormal feature statistics. This observation raises a concern that the effectiveness of *i*-LN could diminish as the network width is expanded. To test the robustness

of i -LN, we increase the network’s capacity and accordingly, also the number of training iterations. We then compare the performance improvements in Tab.3 (Idx 1–3), which indicates that i -LN not only retains its benefits but may also achieve greater performance gains in this expanded setting. This experiment suggests that feature divergence is an issue beyond mere capacity under-utilization.

4.2.4 Channel Imbalance and Bias Alignment

Earlier, we observed extreme feature norms and imbalances in channel entropy, indicating highly peaky feature distributions concentrated in specific channels. Interestingly, despite these severe imbalances, baseline IR Transformers manage to converge and produce outputs with well-bounded magnitudes. To investigate this paradox, we visualize the unnormalized feature scales along the channel dimension before the final normalization layer and compare them with learned biases across various IR tasks (Fig. 7).

We observe sharp peaks in the bias parameters precisely aligning with the channels exhibiting high magnitudes. This exact alignment reveals a compensatory mechanism where the learnable affine terms (γ, β) of LayerNorm counteract abnormal channel activations, allowing baselines to yield normal images. Additionally, this also indicates that the normalization operation (μ, σ) itself is incapable of directly removing these extreme peaks. Moreover, this provide insight into how IR transformers effectively bypass LayerNorm by amplifying values of specific channels. In Sec.4.2.7, we further highlight practical implications where these extreme internal feature magnitudes themselves become critically problematic, particularly, reduced-precision inference scenarios.

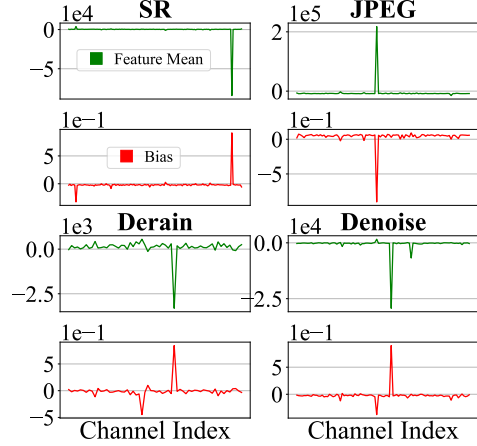


Figure 7: Exact alignment between learned bias parameters (β) and channel-wise feature magnitudes, highlighting a compensatory mechanism observed near the network output.

4.2.5 Empirical Study on Rescale

Although normalization stabilizes training, it also removes input-dependent variations essential for accurate image reconstruction. We ablate the rescaling strategy in our i -LN, which is indicated as LN*, and investigate its empirical effects. As shown in rows 2–3 of Table 3, ablating the proposed rescaling leads to overall performance drop. We also analyzed the effect of rescaling in terms of channel-axis entropy (Fig. 8). The results indicate that rescaling further stabilizes feature entropy, indicating better-distributed activations across the channels. These support the importance of effectively preserving input-specific statistics, enabling the network to gain flexibility when modeling intrinsic features. However, even when rescaling is omitted, we still outperform the baseline normalization in quantitative scores (row 1 of Table 3) and stability in entropy (Fig. 8) due to our spatially holistic normalization, which better preserves the inter-token relationship than traditional per-token normalization schemes.

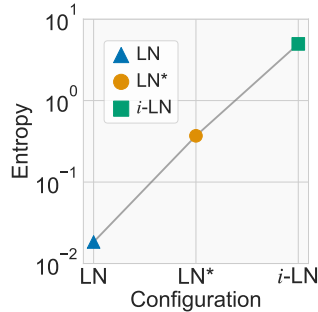


Figure 8: Entropy change for each normalization scheme.

4.2.6 Enhanced Spatial Correlation via Structured RPE

Relative Position Embeddings (RPE) explicitly encodes relative spatial positions between tokens in an input-agnostic manner, similar to the convolution operation that inherently captures the spatial locality through their structured kernel patterns. Accordingly, we can consider well-structured RPEs as a strong indicator of enhanced spatial correlation understanding. In Fig.9, we analyze how our proposed normalization method influences spatial relationship modeling by visualizing the learned RPE of both the baseline IR Transformer and our proposed method. The baseline Transformer exhibits noisy, unstructured embedding patterns, suggesting a limited capability to effectively model spatial correlations. Conversely, our method produces RPEs that resemble well-structured convolutional filter patterns, clearly indicating superior capture of spatial relationships. This structured embedding aligns with our hypothesis that our spatially holistic normalization better preserves intrinsic spatial correlations, helping the network to learn spatial relations more effectively.

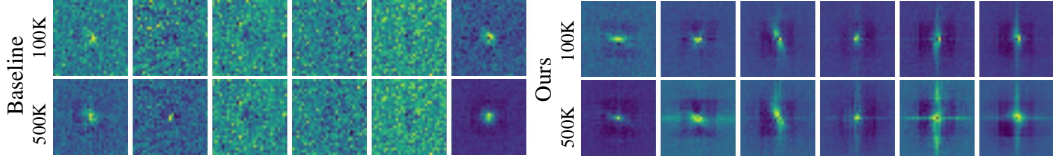


Figure 9: Visualization of Relative Position Embeddings (RPE) per head. Ours exhibit well-structured RPEs, indicating the superiority in understanding the spatial relationship between pixels.

Idx	Backbone	BSD100		Urban100	Manga109
1	HAT [†] + LN	27.7897		26.8779	31.5444
2	HAT [†] + <i>i</i> -LN	27.9206		27.5849	32.1694
3	HAT [†] + LN*	27.9034		27.5335	32.0837
Idx	Backbone	Quantization		Urban100	Manga109
4	HAT [†] + LN	W	int8	26.8711	31.5266
5	HAT [†] + <i>i</i> -LN	W	int8	27.5818	32.1657
6	HAT [†] + LN	W	int4	25.0242	28.0831
7	HAT [†] + <i>i</i> -LN	W	int4	26.8292	30.6596
8	HAT [†] + LN	W+F	fp16	7.4640	5.0736
9	HAT [†] + <i>i</i> -LN	W+F	fp16	27.5849	32.1693

Table 3: Quantitative results for $\times 4$ SR. [†] indicates increased network capacity and longer training. LN* indicates our method without the rescaling strategy. Rows 4–7 apply weights-only (W) quantization, and rows 8–9 use half-precision for both weights and features (W+F fp16).

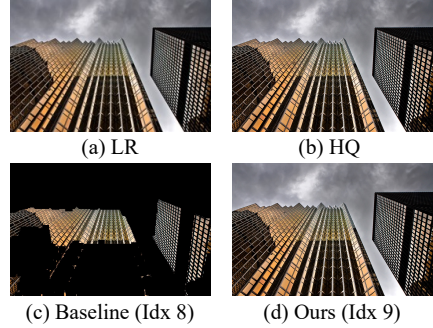


Figure 10: Half-precision inference results for $\times 4$ SR (rows 8–9 in Tab. 3). Baseline (LN) produces artifacts (black dots) due to FP16 overflow; ours remains artifact-free with zero fidelity loss.

4.2.7 Low Precision Inference

Image restoration networks often require deployment on lightweight edge devices, creating significant demand for efficient inference in IR Transformers. A common approach to enhance inference efficiency is reducing precision during model deployment. Consequently, we conducted experiments under reduced-precision inference conditions to empirically evaluate the effects of *i*-LN. Initially, we applied linear weight quantization to the model weights (Idx 4–7). As shown in Tab.3, vanilla LayerNorm resulted in substantial performance degradation, while *i*-LN demonstrated remarkable stability. We further conducted half-precision inference experiments, casting both internal feature values and weights to half-precision floating-point numbers (Idx 8–9). Fig.10 illustrates that vanilla LayerNorm generated extensive regions of black dots, indicating network-generated infinity values due to extreme internal feature magnitudes inadequate for low-precision conditions. Notably, no substantial performance degradation was observed in regions where the network maintained finite feature values. This highlights the necessity of well-bounded feature values achieved by *i*-LN, emphasizing its critical role in enabling efficient inference for IR Transformers.

5 Conclusion

In this study, we analyze the internal training dynamics of Image Restoration (IR) Transformers, highlighting a critical yet often overlooked phenomenon: significant divergence in feature magnitudes accompanied by collapses in channel-wise entropy. We interpret this behavior from the perspective of networks attempting to bypass constraints imposed by conventional LayerNorm due to a fundamental mismatch between these constraints and the unique demands inherent to IR tasks. Specifically, LayerNorm’s per-token normalization and input-independent scaling disrupt critical spatial correlations and limit essential feature flexibility required for accurate restoration. Accordingly, we introduce Image Restoration Transformer Tailored Layer Normalization (*i*-LN), a simple drop-in replacement for conventional LayerNorm. It is designed to better align with the unique characteristics of IR tasks and preserve important low-level features of the input throughout the network. Our method normalizes across the entire spatial and channel dimensions and incorporates an input-dependent rescaling strategy. Through extensive experiments, we demonstrate that *i*-LN effectively prevents abnormal feature divergence leading to robustness under low-precision inference, and maintains stable channel-wise entropy, and significantly improves IR performance across various IR tasks.

References

- [1] E. Agustsson and R. Timofte. Ntire 2017 challenge on single image super-resolution: Dataset and study. In *Proceedings of the IEEE Conference on Computer Vision and Pattern Recognition Workshops*, pages 126–135, 2017.
- [2] J. L. Ba, J. R. Kiros, and G. E. Hinton. Layer normalization. *arXiv preprint arXiv:1607.06450*, 2016.
- [3] T. Bachlechner, B. P. Majumder, H. Mao, G. Cottrell, and J. McAuley. Rezero is all you need: Fast convergence at large depth. In *Uncertainty in Artificial Intelligence*, pages 1352–1361. PMLR, 2021.
- [4] M. Bevilacqua, A. Roumy, C. Guillemot, and M. L. Alberi-Morel. Low-complexity single-image super-resolution based on nonnegative neighbor embedding. 2012.
- [5] X. Chen, Z. Li, Y. Pu, Y. Liu, J. Zhou, Y. Qiao, and C. Dong. A comparative study of image restoration networks for general backbone network design. In *European Conference on Computer Vision*, pages 74–91. Springer, 2024.
- [6] X. Chen, X. Wang, W. Zhang, X. Kong, Y. Qiao, J. Zhou, and C. Dong. Hat: Hybrid attention transformer for image restoration. *arXiv preprint arXiv:2309.05239*, 2023.
- [7] X. Chen, X. Wang, J. Zhou, Y. Qiao, and C. Dong. Activating more pixels in image super-resolution transformer. In *Proceedings of the IEEE/CVF conference on computer vision and pattern recognition*, pages 22367–22377, 2023.
- [8] C. Dong, C. C. Loy, K. He, and X. Tang. Image super-resolution using deep convolutional networks. *IEEE transactions on pattern analysis and machine intelligence*, 38(2):295–307, 2015.
- [9] A. Dosovitskiy, L. Beyer, A. Kolesnikov, D. Weissenborn, X. Zhai, T. Unterthiner, M. Dehghani, M. Minderer, G. Heigold, S. Gelly, et al. An image is worth 16x16 words: Transformers for image recognition at scale. *arXiv preprint arXiv:2010.11929*, 2020.
- [10] A. Foi, V. Katkovnik, and K. Egiazarian. Pointwise shape-adaptive dct for high-quality denoising and deblocking of grayscale and color images. *IEEE transactions on image processing*, 16(5):1395–1411, 2007.
- [11] R. Franzen. Kodak lossless true color image suite. <http://r0k.us/graphics/kodak>, 1999. Volume 4, no. 2.
- [12] C.-C. Hsu, C.-M. Lee, and Y.-S. Chou. Drct: Saving image super-resolution away from information bottleneck. *arXiv preprint arXiv:2404.00722*, 2024.
- [13] J.-B. Huang, A. Singh, and N. Ahuja. Single image super-resolution from transformed self-exemplars. In *Proceedings of the IEEE conference on computer vision and pattern recognition*, pages 5197–5206, 2015.
- [14] S. Ioffe and C. Szegedy. Batch normalization: Accelerating deep network training by reducing internal covariate shift. In *International conference on machine learning*, pages 448–456. pmlr, 2015.
- [15] K. Jiang, Z. Wang, P. Yi, C. Chen, B. Huang, Y. Luo, J. Ma, and J. Jiang. Multi-scale progressive fusion network for single image deraining. In *Proceedings of the IEEE/CVF conference on computer vision and pattern recognition*, pages 8346–8355, 2020.
- [16] T. Karras, M. Aittala, J. Lehtinen, J. Hellsten, T. Aila, and S. Laine. Analyzing and improving the training dynamics of diffusion models. In *Proceedings of the IEEE/CVF Conference on Computer Vision and Pattern Recognition*, pages 24174–24184, 2024.
- [17] T. Karras, S. Laine, M. Aittala, J. Hellsten, J. Lehtinen, and T. Aila. Analyzing and improving the image quality of stylegan. In *Proceedings of the IEEE/CVF conference on computer vision and pattern recognition*, pages 8110–8119, 2020.

- [18] J. Kim, J. K. Lee, and K. M. Lee. Accurate image super-resolution using very deep convolutional networks. In *Proceedings of the IEEE conference on computer vision and pattern recognition*, pages 1646–1654, 2016.
- [19] J. Liang, J. Cao, G. Sun, K. Zhang, L. Van Gool, and R. Timofte. Swinir: Image restoration using swin transformer. In *Proceedings of the IEEE/CVF International Conference on Computer Vision*, pages 1833–1844, 2021.
- [20] B. Lim, S. Son, H. Kim, S. Nah, and K. M. Lee. Enhanced deep residual networks for single image super-resolution. In *The IEEE Conference on Computer Vision and Pattern Recognition (CVPR) Workshops*, July 2017.
- [21] B. Lim, S. Son, H. Kim, S. Nah, and K. Mu Lee. Enhanced deep residual networks for single image super-resolution. In *Proceedings of the IEEE conference on computer vision and pattern recognition workshops*, pages 136–144, 2017.
- [22] Z. Liu, Y. Lin, Y. Cao, H. Hu, Y. Wei, Z. Zhang, S. Lin, and B. Guo. Swin transformer: Hierarchical vision transformer using shifted windows. In *Proceedings of the IEEE/CVF international conference on computer vision*, pages 10012–10022, 2021.
- [23] D. Martin, C. Fowlkes, D. Tal, and J. Malik. A database of human segmented natural images and its application to evaluating segmentation algorithms and measuring ecological statistics. In *Proceedings Eighth IEEE International Conference on Computer Vision. ICCV 2001*, volume 2, pages 416–423. IEEE, 2001.
- [24] Y. Matsui, K. Ito, Y. Aramaki, A. Fujimoto, T. Ogawa, T. Yamasaki, and K. Aizawa. Sketch-based manga retrieval using manga109 dataset. *Multimedia Tools and Applications*, 76:21811–21838, 2017.
- [25] H. Sheikh. Live image quality assessment database release 2. <http://live.ece.utexas.edu/research/quality>, 2005.
- [26] H. Touvron, M. Cord, A. Sablayrolles, G. Synnaeve, and H. Jégou. Going deeper with image transformers. In *Proceedings of the IEEE/CVF international conference on computer vision*, pages 32–42, 2021.
- [27] D. Ulyanov, A. Vedaldi, and V. Lempitsky. Instance normalization: The missing ingredient for fast stylization. *arXiv preprint arXiv:1607.08022*, 2016.
- [28] X. Wang, C. Dong, and Y. Shan. Repr: Training efficient vgg-style super-resolution networks with structural re-parameterization and batch normalization. In *Proceedings of the 30th acm international conference on multimedia*, pages 2556–2564, 2022.
- [29] X. Wang, K. Yu, S. Wu, J. Gu, Y. Liu, C. Dong, Y. Qiao, and C. Change Loy. Esrgan: Enhanced super-resolution generative adversarial networks. In *Proceedings of the European conference on computer vision (ECCV) workshops*, pages 0–0, 2018.
- [30] Z. Wang, X. Cun, J. Bao, W. Zhou, J. Liu, and H. Li. Uformer: A general u-shaped transformer for image restoration. In *Proceedings of the IEEE/CVF conference on computer vision and pattern recognition*, pages 17683–17693, 2022.
- [31] W. Yang, R. T. Tan, J. Feng, J. Liu, Z. Guo, and S. Yan. Deep joint rain detection and removal from a single image. In *Proceedings of the IEEE conference on computer vision and pattern recognition*, pages 1357–1366, 2017.
- [32] S. W. Zamir, A. Arora, S. Khan, M. Hayat, F. S. Khan, and M.-H. Yang. Restormer: Efficient transformer for high-resolution image restoration. In *Proceedings of the IEEE/CVF conference on computer vision and pattern recognition*, pages 5728–5739, 2022.
- [33] R. Zeyde, M. Elad, and M. Protter. On single image scale-up using sparse-representations. In *International conference on curves and surfaces*, pages 711–730. Springer, 2010.
- [34] B. Zhang and R. Sennrich. Root mean square layer normalization. *Advances in Neural Information Processing Systems*, 32, 2019.

- [35] D. Zhang, F. Huang, S. Liu, X. Wang, and Z. Jin. Swinfir: Revisiting the swinir with fast fourier convolution and improved training for image super-resolution. *arXiv preprint arXiv:2208.11247*, 2022.
- [36] H. Zhang, V. Sindagi, and V. M. Patel. Image de-raining using a conditional generative adversarial network. *IEEE transactions on circuits and systems for video technology*, 30(11):3943–3956, 2019.
- [37] L. Zhang, X. Wu, A. Buades, and X. Li. Color demosaicking by local directional interpolation and nonlocal adaptive thresholding. *Journal of Electronic imaging*, 20(2):023016–023016, 2011.
- [38] Y. Zhang, K. Li, K. Li, L. Wang, B. Zhong, and Y. Fu. Image super-resolution using very deep residual channel attention networks. In *Proceedings of the European conference on computer vision (ECCV)*, pages 286–301, 2018.